Investigation of Cue-Based Aggregation Behaviour in Complex Environments

Shiyi Wang[1], Ali E. Turgut[2], Thomas Schmickl[3], Barry Lennox[1], and Farshad Arvin[1(✉)]

[1] Swarm and Computational Intelligence Lab (SwaCIL), Department of Electrical and Electronic Engineering, The University of Manchester, Manchester, UK
{shiyi.wang,farshad.arvin}@manchester.ac.uk
[2] Department of Mechanical Engineering, Middle East Technical University, Ankara, Turkey
[3] Artificial Life Lab, Institute of Biology, University of Graz, Graz, Austria

Abstract. Swarm robotics is mainly inspired by the collective behaviour of social animals in nature. Among different behaviours such as foraging and flocking performed by social animals; aggregation behaviour is often considered as the most basic and fundamental one. Aggregation behaviour has been studied in different domains for over a decade. In most of these studies, the settings are over-simplified that are quite far from reality. In this paper, we investigate cue-based aggregation behaviour using BEECLUST in a complex environment having two cues –one being the local optimum and the other being the global optimum– with an obstacle between the two cues. The robotic validation of the BEECLUST strategy in a complex environment is the main motivation of this paper. We measured the aggregation size on both cues with and without the obstacle varying the number of robots. The simulations were performed on a custom open-source simulation platform, *Bee-Ground*, using *MONA* robots. The results showed that the aggregation behaviour with BEECLUST strategy was able to overcome a certain degree of environmental complexities revealing the robustness of the method. We also verified these results using our stock-flow model.

Keywords: Swarm robotics · Aggregation · BEECLUST

1 Introduction

Aggregation is a common behaviour observed in different species ranging from amoeba to insects [11]. In aggregation individuals of a species gather in one area with or without an environmental cue [16]. Aggregation is the basis and a prerequisite for many complex swarm tasks, e.g. flocking and foraging [10,27]. There are two types of aggregation behaviour in nature: cue-based aggregation and self-organised aggregation [11]. In cue-based aggregation, there is a cue present in

H. Gao et al. (Eds.): CollaborateCom 2020, LNICST 350, pp. 18–36, 2021.
https://doi.org/10.1007/978-3-030-67540-0_2

the environment where animals gather [8]. The cue represents the optimal location in terms of temperature, humidity or such. For example, young honeybees tend to gather in optimal areas with temperatures between 34 °C and 38 °C [17] while flies gather in hot and humid locations [14]. Hence, in cue-based aggregation environment plays a very important role and in most cases, environment is very complex having multiple cues, obstacles and predators that animals have to tackle. These make aggregation a very challenging task even for the animals. In self-organised aggregation, there is no cue in the environment. Animals gather in random locations without any particular external cue in the environment [15].

Researchers in swarm robotics study aggregation behaviour to better understand aggregation behaviour in biology [29] or to replicate it artificially with robots [8] since aggregation behaviour is the basis of most of the behaviours in swarm robotics [8,10,25,27,33]. Among different approaches, BEECLUST algorithm proposed by Schmickl et al. [29] that mimics the thermotaxis behaviour of honeybees is one of the simple yet a very elegant approach to cue-based aggregation in swarm robots.

Cue-based aggregation in swarm robotics can be traced back to the 1990s with Kube and Zhang's [22] pioneering experiment on robot aggregation around a light source. Since then, there have been many studies such as [18] proposing an aggregation scenario based on the infrared transmitter. In a recent study on the effects of environmental changes on the performance of swarm robotic aggregation [8] using real mobile robots, it has been shown that the BEECLUST algorithm is an efficient mechanism for cue-based aggregation with optimal performance in dynamic and complex environments. The study also proposed a probabilistic aggregation model to represent the influence of swarm parameters, e.g. population and arena size, on the aggregation size. Another study [30] proposed two macroscopic models based on the BEECLUST algorithm to predict the aggregation behaviour in a dynamic environment. Mathematical modelling is an efficient tool for predicting the behaviour of a swarm system. It is used to predict the collective behaviour of a group by analysing the random behaviour of the individuals [32]. In other studies [13,19,20], different models for predicting the macroscopic behaviour of swarms have been proposed. Another study [21] proposed a mathematical model which can account for peculiarities of energy transfer among swarm robots. In addition, modelling approaches from other research fields have also been used to study the modelling of swarm robotics problems. One such research study [23] used a chemical reaction network to model the interaction between individuals in robot swarms. In another study [30], *Stock-Flow* model was used, borrowed from macro-economics, to predict the performance of a cue-based swarm aggregation.

Most of the previous studies which are based on real-robot implementations used small swarm populations, and the duration of the experiments were very limited [4,8,25]. There are relatively few studies on the aggregation of swarm robots in a complex environment with multiple cues and obstacles. In this paper, we studied the aggregation of large number of robots using BEECLUST algorithm in an environment with two cues having different intensities and an

obstacle. We investigated the effects of the environmental factors on aggregation. The robotic validation of the BEECLUST strategy in a complex environment is the main motivation of this paper. We also improved a mathematical model [30] and used it to predict the aggregation size on different settings. The simulation was based on the open-sourced robot MONA [3] and open-sourced simulation platform Bee-Ground [1].

The rest of this paper was structured as follows: in Sect. 2, we introduced the aggregation method. In Sect. 3, the stock-flow model was discussed. In Sect. 4, we presented the realisation of aggregation using Bee-Ground. In Sect. 5, we discussed the results of the experiments. In Sect. 6, we concluded the paper and discussed future research directions.

2 Aggregation Method

The aggregation method used in this study is based on BEECLUST [31]. It imitates the thermotaxis behaviour of young bees that aggregate at an optimal zone with temperature between 34 °C to 38 °C. Previous studies demonstrated that the BEECLUST algorithm successfully imitates the aggregation behaviour of bees on the optimal zone [6,8,9,28]. In most cases, the cue has been modelled by a light or sound source instead of a heat source due their simplicity in implementaion.

Based on the BEECLUST algorithm (depicted in Fig. 1), a robot moves forward in the environment until it encounters an object. It checks if the object is an obstacle or another robot.

- If it is an obstacle, the robot turns to avoid the obstacle and moves forward.
- If it is another robot, it stops and waits for a particular amount of time. The waiting time $w(t)$ in Eq. (1) depends on intensity of the cue. The stronger cue results in a longer waiting time.

When the waiting time finishes, the robot turns randomly and moves forward again. The waiting time, $w(t)$, is calculated by:

$$w(t) = w_{max} \cdot \frac{S(t)^2}{S(t)^2 + \mu}. \tag{1}$$

The waiting time, Eq. (1), was adopted from the previous studies [5]. $S(t)$ denotes the sensory reading. The sensor range is from 0 and 255. w_{max} is the maximum waiting time, and μ is a parameter which changes the steepness of the waiting curve. The constants w_{max} and μ were chosen empirically: $w_{max} = 60\,\mathrm{s}$ and $\mu = 5000$.

3 The Stock-Flow Model

The origin of the stock-flow model can be traced to work in the mid-twentieth century. It was used to study the dynamic relationship between the flow of

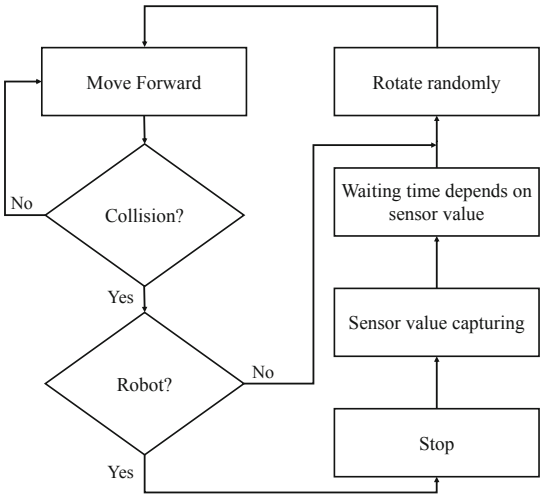

Fig. 1. Flowchart of the BEECLUST aggregation algorithms

income and expenditure and changes in national assets in the US economy [12]. In a recent work [30], this model was used to predict the aggregation of swarm robots in presence of two cues.

To model the aggregation behaviour in this study, we adopted the proposed model in [30] and used Vensim^{TM} [2] software for the numerical modelling. In this model, 'stock' is the total number of robots in the arena.

These robots can be divided into three aggregation states, 1) the number of free robots $F(t)$, 2) the number of robots aggregated on the left source (weak source) at time t is $A_{left}(t)$, and 3) the number of robots aggregated on the right source at time t is $A_{right}(t)$. This is a constant value that does not change over time. The structure of our model is depicted in Fig. 2.

We have two sources hence two aggregations in our setting. The robots shift between each states at a certain rate. The rate at which robots join the aggregation on the left source at time t is $J_{left}(t)$. Meanwhile, the rate at which robots leave the aggregation on the left source at time t is $L_{left}(t)$.

Therefore, the rate of change the number of robots on the left source is:

$$\frac{A_{left}(t)}{dt} = J_{left}(t) - L_{left}(t). \tag{2}$$

The leave rate $L_{left}(t)$ can be described as:

$$L_{left}(t) = \frac{A_{left}(t)}{w_{left}(t)}. \tag{3}$$

$w_{left}(t)$ is the waiting time for a single robot on the left source at time t, which depends on the sensor value $S(t)$ obtained at the position where the robot stopped moving.

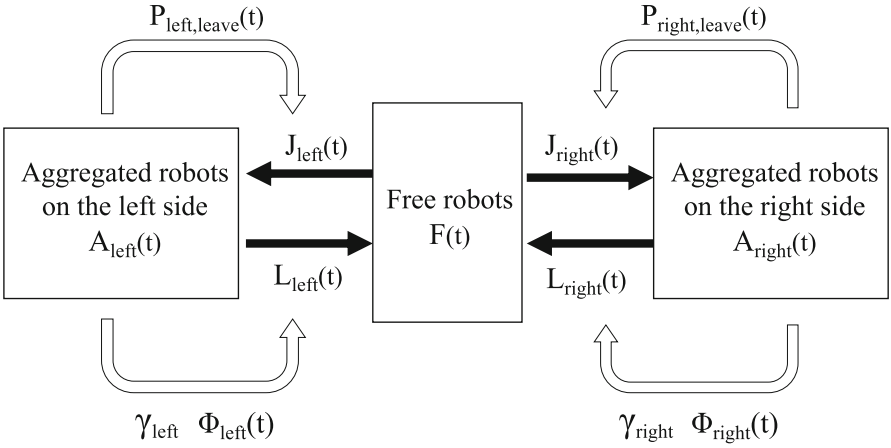

Fig. 2. Developed Stock-Flow model for aggregation

We modeled $L_{left}(t)$ with slight changes to the previous model proposed in [30]. The applied changes showed improvement in predicting the system, due to the following reasons:

1. After the waiting time is over, the robots randomly turn at an angle and continue moving forward. However, there is a high probability for at least one of them to stop immediately again. This occurs when both robots face each other again after a random rotation, or one of them face the other robots in the aggregation. Therefore, their position would not change at this moment and the robot can not leave the aggregation.
2. In more complicated situations in a large aggregation, the internal robots near the centre of the aggregation are not able to leave the group regardless of turning angles. This is because of the surrounding robots that are still in their waiting period.

In our model, we used a function $P_{leave}(t)$ to describe the probability of which robots can leave the aggregation which based on the size of the aggregation. In this paper, the function $P_{left,leave}(t)$ is the probability of which robots can leave the left aggregation. We fitted the function $P_{left,leave}(t)$ based on the observed results [4,7] from preliminary experiments. It is calculated as:

$$P_{left,leave}(t) = 0.25 * (-(\frac{\pi}{2})^{-1} \arctan(\frac{A_{left}(t)}{100} - 3.5) + 1) \, . \tag{4}$$

The rate $L_{left}(t)$ in our model is described as:

$$L_{left}(t) = P_{left,leave}(t) \frac{A_{left}(t)}{w_{left}(t)}. \tag{5}$$

Moreover, the joining rate $J_{left}(t)$ which is calculated from the number of robots which join the aggregation on the left hand side per second at time t is calculated by:

$$J_{left}(t) = \gamma_{left} F(t) \Phi_{left}(t) P_{detect}, \tag{6}$$

where γ_{left} is a fraction of a free robot appearing in the left hand side of the arena assuming that free robots are evenly distributed and $\Phi_{left}(t)$ is the probability of a robot meeting another robot in the arena. The area of the arena on the left hand side is 65.4% of the total arena, while the right-hand side area is 34.6% of the total arena. Thus, $\gamma_{left} = 65.4\%$.

$F(t)$ is the total number of free robots in the arena. P_{detect} is the probability of a robot to identify a robot-to-robot collision which is assumed:

$$P_{detect} = 0.5. \tag{7}$$

On the other hand, $\Phi_{left}(t)$ can be calculated through geometric considerations, mainly the ratio of the area covered by the robots to the total area of arena.

The area covered by a single robot is:

$$k_{aggr} = \pi r_{robot}^2. \tag{8}$$

The space covered by a free moving robot in time t is related to its speed and area, which is described by:

$$k_{mov}(t) = \pi r_{robot}^2 + 2 r_{robot} v t, \tag{9}$$

where v represents the robots' speed ($v = 0.02$ m/s).

We assume that the free robots are evenly distributed across the arena, so the number of the free robots in the left side is $\gamma_{left} F(t)$.

Therefore,

$$\Phi_{left}(t) = \frac{\gamma_{left} F(t) k_{mov}(t) + A_{left}(t) k_{aggr}}{\gamma_{left} k_{arena}}, \tag{10}$$

where k_{arena} represents the total area of the arena.

The probabilities for the right-hand side of the arena are calculated similar to the left-hand side. Hence, the change rate of the free moving robots $F(t)$ in the arena can be described as:

$$F(t) = L_{left}(t) + L_{right}(t) - J_{left}(t) - J_{right}(t). \tag{11}$$

4 Experimental Setup

4.1 Simulation Platform

We developed a simulation platform, *Bee-Ground*, on Unity real-time development platform and using an open-source tool, Unity Machine Learning Agents.

Compare to other mainstream robotic simulation platforms such as ARGoS [26], Webot [24], Stage [34], Bee-Ground is able to simulate long-term operations of swarm robots in various complex and dynamic environments including obstacles and multiple sources. This is because it performs multi-layer and multi-scenario simulations simultaneously 40 times faster than the real-time without losing sampling resolution. Moreover, thanks to the built-in physics engines in Unity, our simulation platform, *Bee-Ground*, can realistically reproduce the operation of multiple robots in complex environments.

Figure 3 illustrates a randomly selected aggregation experiments with an obstacle between two sources.

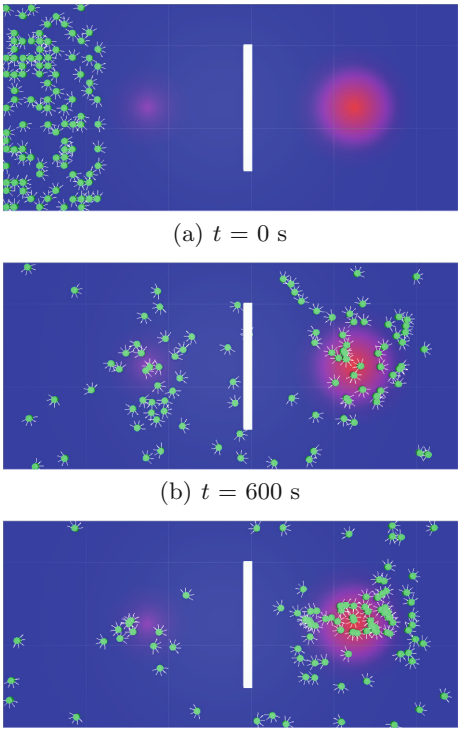

(a) $t = 0$ s

(b) $t = 600$ s

(c) $t = 3600$ s

Fig. 3. A sample simulation in Bee-Ground with swarm population of $N = 200$ robots in obstacle size with 60% of arena width. The right-hand side cue is the global optimal and the left hand side cue is a local optimum.

All experimental parameters, e.g. arena dimensions, obstacles' configuration and sources are defined by input array files. In this paper, we used a model of MONA robot [3] as shown in Fig. 4.

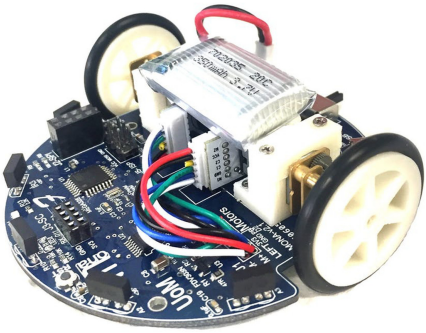

Fig. 4. Mona - an open-source robotic platform for swarm robotics.

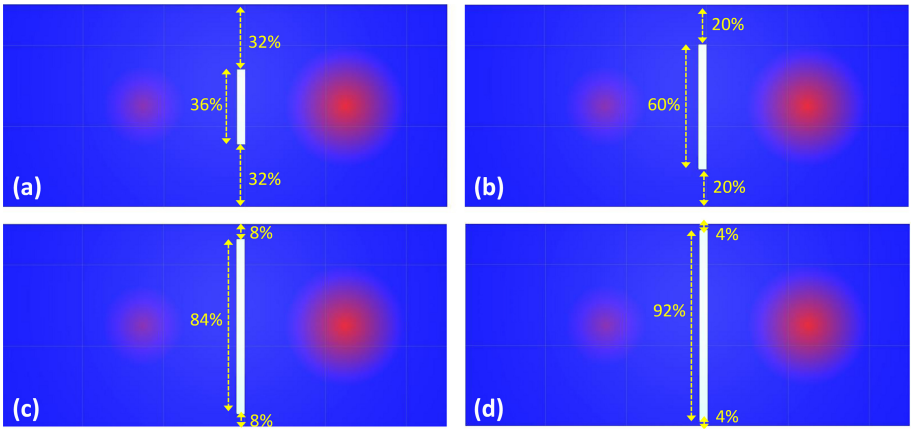

Fig. 5. Four different obstacle sizes in Bee-Ground with $\{36\%, 60\%, 84\%, 92\%\}$ of arena width.

4.2 Arena Setup

The arena size was 440 cm in length and 200 cm in width. It was surrounded by walls which stop the robots from moving out of the arena. An obstacle with different lengths were set up in the middle of the arena between the two sources. In this paper, we used five different obstacle lengths, $L_o \in \{0, 72, 120, 168, 184\}$ cm corresponding to no-obstacle, 36%, 60%, 84% and 92% of arena width, respectively (Fig. 5).

Two gradient-based heat sources were utilised as cues in this study (Fig. 3). The one on the left side, the local optimum, had a temperature of 125 unit (out of 255) at the centre point with a radius of 40 cm. The heat source on the right-hand side, the global optimal, had a temperature of 255 unit (out of 255) at the centre point with a radius of 60 cm.

4.3 Initialisation

All the robots were randomly placed on the left side of the arena to keep them away from the global optimal. They moved according to the BEECLUST algorithm during the simulations. Each simulation lasted for 3600 s and all the experiments were repeated 20 times. Table 1 shows the list of parameters and variables were used in this study.

Table 1. Parameter of Experiments

Parameter	Description	Range/Value
L_a	Length of arena	440 cm
W_a	Width of arena	200 cm
L_o	Length of obstacles	{72, 120, 168, 184} cm
W_o	Width of obstacles	8 cm
r_{cL}	Radius of the left cue	40 cm
r_{cR}	Radius of the right cue	60 cm
r_r	Radius of robot	3.25 cm
v_r	Robot forward speed	2 cm/s
ω_{turn}	Turning speed	1 rad/s
r_s	Radius of robot IR sensory system	8 cm
t_w	Waiting Time after collision	0 to 60 s

4.4 Experimental Configurations

We implemented aggregation with two different settings, without an obstacle and with a variable size obstacles.

Without Obstacles. In this setting, a group of $N \in \{100, 150, 200, 250, 300\}$ robots were deployed. At the beginning, the robots were randomly placed on the left side of the arena. We tracked the number of robots which are aggregated on both left and right-hand cues during the experiments.

With Obstacles. In this setting, $N = \{200, 300\}$ robots were used. We also set four different obstacle sizes—36% ($L_o = 72$ cm), 60% ($L_o = 120$ cm), 84% ($L_o = 168$ cm) and 92% ($L_o = 184$ cm)—sequentially. We observed the size of aggregations on both cues.

5 Results

In both configuration, the solid orange lines in the graphs show the median value of the number of robots that were aggregated on the main cue (global optimum

on the right-hand side). The orange shades in each population indicate the lower quartile value to the upper quartile value. Also, the solid blue lines in the graphs show the median value of the number of robots that were aggregated on the weak cue (local optimum on the left side). The blue shades indicate the lower quartile value to the upper quartile value.

5.1 Without Obstacles

Figure 6 illustrates aggregation size on the main cue from experiments without obstacle. The five simulations showed a similar trend. The number of robots in the main aggregation increased to a stable value monotonically. Increasing the number of robots increased the size of aggregation. However, there was a significant difference in the time they reached the final number of aggregations. The group of $N = 300$ robots took approximately 910 s to reach 70% of the final aggregation size on the main cue (right-hand side). Meanwhile, the group of $N = 100$ robots took approximately 400 s to reach 70% of the final aggregation size on the main cue. The time had an approximate exponential relationship with the total swarm size.

It was not obvious, however worth mentioning that the ratio at which the final aggregation size to the total number of robots ($\frac{A_{right}}{N}$) increased slightly as the number of robots increased (Fig. 6).

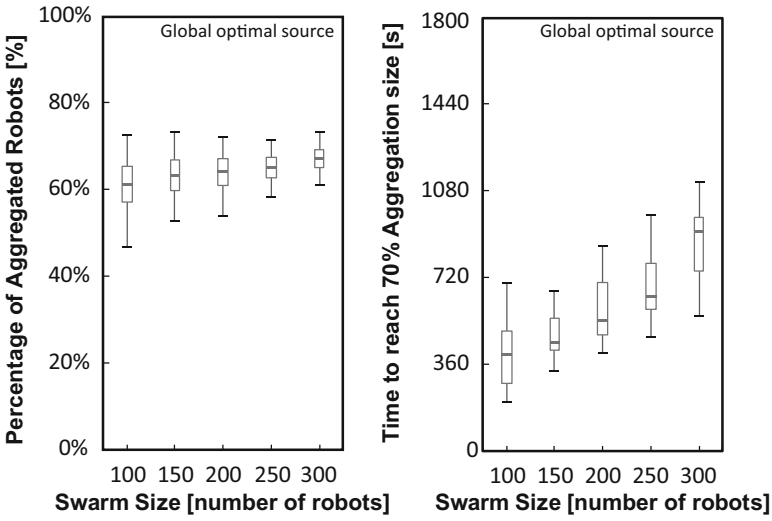

Fig. 6. Ratio of aggregated robots and the time to reach 70% aggregation size of $N = \{100, 150, 200, 250, 300\}$ robots without obstacles at global optimal source

Figure 7 shows the observed aggregation size on the main cue during 3600 s experiments with different population sizes N. Also, the predicted values from the our model were indicated with grey colour dashed lines.

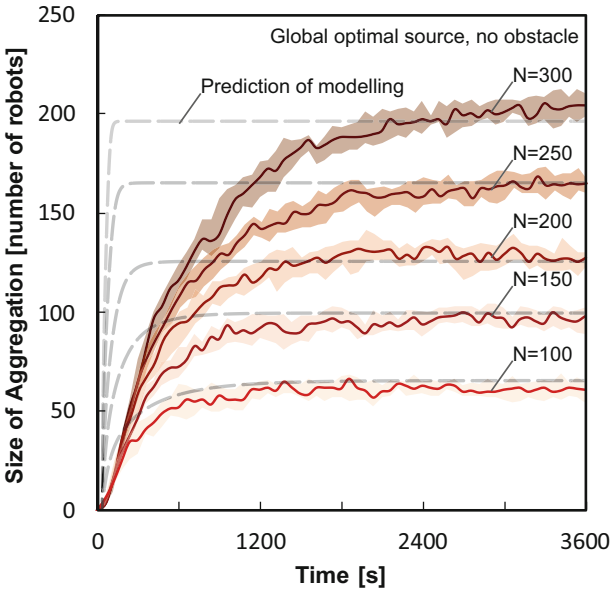

Fig. 7. Size of aggregation at the global optimal source with swarm population of $N = \{100, 150, 200, 250, 300\}$ robots without obstacles

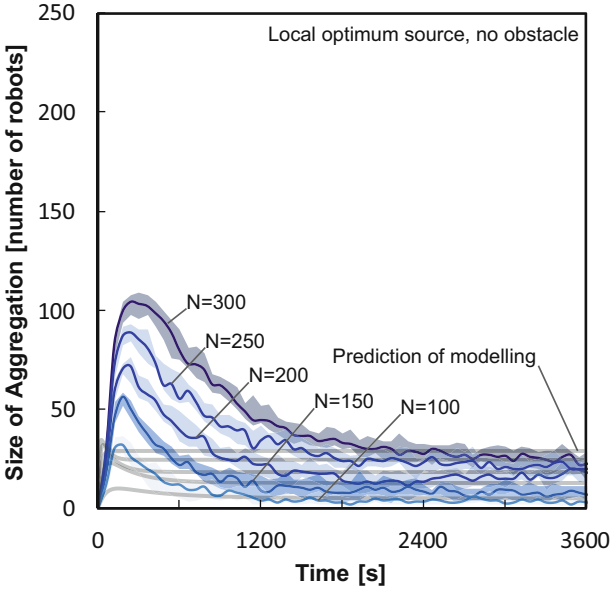

Fig. 8. Size of aggregation at the local optimum source with swarm population of $N = \{100, 150, 200, 250, 300\}$ robots without obstacles

Figure 8 illustrates the size of aggregation on the small cue (left hand size) during 3600 s. The results revealed that the situation in the local optimum source was more complex. In the beginning, the number of robots aggregated in this area reached a peak and then fell back to a stable value (minimum size) which was not shown on the right-hand side cue (in Fig. 7). There was a proportional relationship between the aggregation sizes and the number of robots in the first half time of the experiments. However, as the size of the aggregation stabilized, this proportional relationship gradually disappeared or became less obvious. The observed results show that in the simulation of $N \in \{200, 250, 300\}$ robots, the final sizes of the aggregation were almost the same. There was also no significant difference between $N \in \{100, 150\}$ robots.

5.2 With Obstacles

Figure 9 illustrates the size of aggregation with $N = 200$ robots in experiments with different obstacle sizes of $L_o \in \{36\%, 60\%, 84\%, 92\%\}$ of arena width. The grey dotted lines show the aggregation results in a no-obstacle environment with the same number of robots in each group (as the control). In the global optimal source, we found that the size of the obstacles affected the aggregation time; the larger the obstacle, the longer it took the robots to aggregate. In the arena divided by obstacles with 36% and 60% of the arena width, the final aggregation size reached a stable value that was almost the same as that in the no-obstacle arena. In arenas divided by 84% and 92% obstacles, the aggregation size increased very slowly and did not reach a stable value within the duration of 3600 s.

Figure 10 shows the aggregation size during 3600 s on the left cue (local optimum). It was found that the size of the obstacle affected the peak value of the aggregation size. Hence, in the experiments with the obstacles of 92% of the arena width, the number of aggregated robots was close to the maximum number of robots that could be aggregated in this area. Aggregation size and obstacle length had an inverse relationship, which the number of aggregated robots decreased as the obstacle size increased. In the arena divided by obstacles with 36% and 60% of the arena width, the final aggregation size was the same as in the no-obstacle area. However, in experiments with longer obstacles, 84% and 92% of the arena width, a stable value in the $N = 200$ robots was doubled and trebled as the others.

Figure 11 reveals the aggregation size for $N = 300$ robots with different obstacle sizes. The results were almost similar to the aggregation size observed with $N = 200$ robots.

Similarly, Fig. 12 shows the size of aggregation on the local optimum (left side cue) for experiment with $N = 300$ robots in presence of different obstacles lengths. Results from 36% and 60% showed a similar behaviour as shown in results with $N = 200$ robots.

However, in two extremely difficult situations with the obstacles lengths of 84% and 92% of the arena width, we did not expect that robots can successfully aggregate at the global optimal source during the $t = 3600$ s experiments.

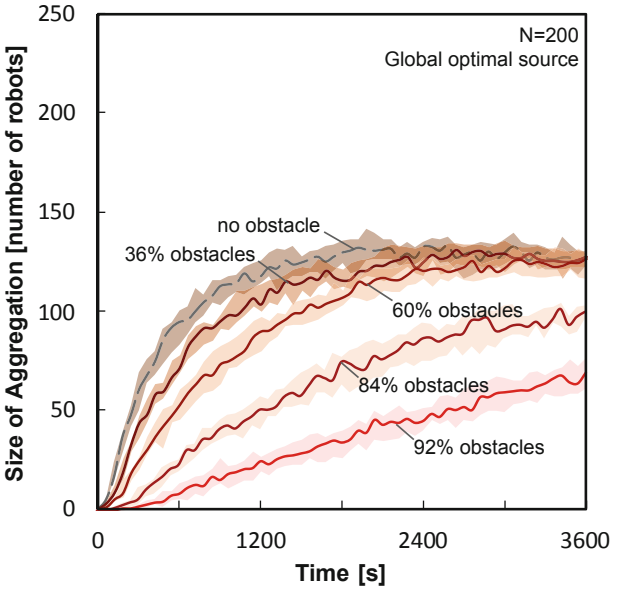

Fig. 9. Size of aggregation at the global optimal source with population of $N = 200$ robots in obstacle sizes with $\{36\%, 60\%, 84\%, 92\%\}$ of arena width

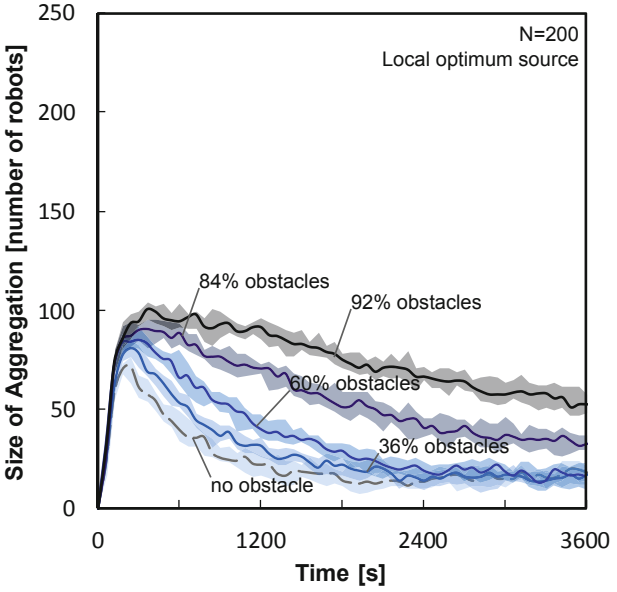

Fig. 10. Size of aggregation at the local optimum source with population of $N = 200$ robots in obstacle sizes with $\{36\%, 60\%, 84\%, 92\%\}$ of arena width.

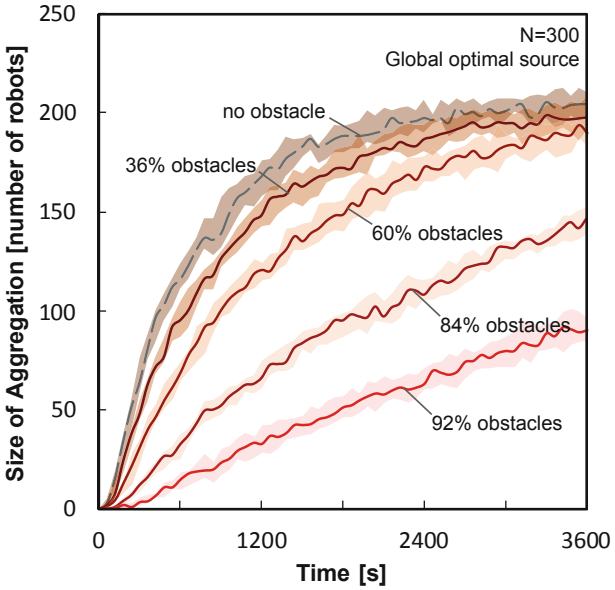

Fig. 11. Size of aggregation at the global optimal source with population of $N = 300$ robots in obstacle sizes with $\{36\%, 60\%, 84\%, 92\%\}$ of arena width.

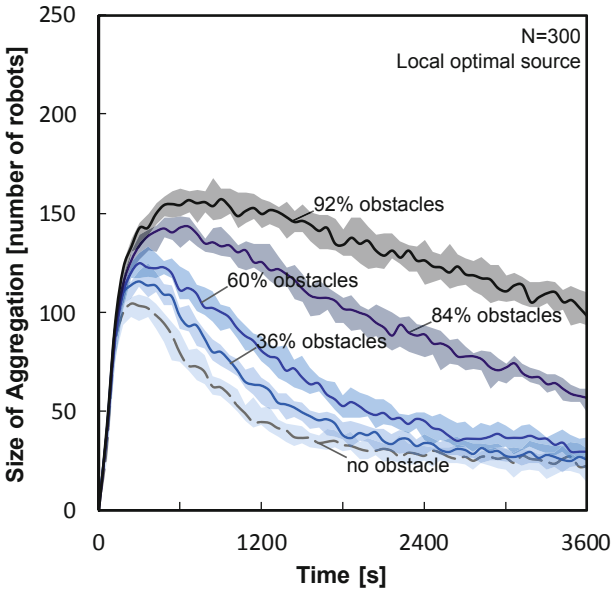

Fig. 12. Size of aggregation at the local optimum source with population of $N = 300$ robots in obstacle sizes with $\{36\%, 60\%, 84\%, 92\%\}$ of arena width.

Therefore, we just calculated the ratio in which robots overcame the obstacles. In experiments with $N = 200$ robots, 44.5% robots (89 of 200 robots) overcame the obstacles in 84% of the arena width. Meanwhile, this ratio in case of $N = 300$ robots is 39.7% (119 of 300 robots). The similar situation observed in the experiments with obstacles in 92% of the arena width in both groups. The ratios were 19% (38 of 200 robots) and 14.3% (43 of 300 robots) respectively.

6 Discussion

6.1 Arena Without Obstacles

Each group of our simulations showed that the global optimal source could eventually attract more robots to aggregate than the local optimum source. Although the capability of BEECLUST in finding the global optimum was demonstrated, the speed and efficiency of completing the aggregation were different. The total number of robots affected the aggregation speed in the global optimal source. The larger the number of robots, the slower the gathering speed of the robot. It is due to increase in number of inter-robot collisions.

In our stock-flow model, we discussed the $P_{leave}(t)$ function, the probability that a robot leaves an aggregation. It changed as the size of the aggregation changed. The larger the aggregation, the lower the probability that the robot would leave, and vice versa. Therefore, it was found that when there were two cues in the arena, the larger cue reduced the aggregation ability of the smaller cue because of the change of this probability because of the following reasons:

- As the size of aggregation in the bigger cue grows, free robots have a higher probability of entering larger aggregation. This probability increases continuously. As a result, more robots join and the number of free robots becomes smaller.
- Also, the rate at which robots enter the smaller cue becomes smaller. Each robot that leaves the smaller cue has a higher probability of joining the aggregation in the bigger cue. Hence, the aggregation size in the smaller cue decreases continuously results in the rate at which robots leave it increases.

Our model's prediction and simulation results of the aggregation size were close. The difference was at the beginning of the experiments, that was, the robots' initialisation position. In the model, we set the robots in random positions uniformly, however, we initialised the robots on the left hand side.

We found that the probability of a robot leaving the aggregation had a significant effect on the aggregation results in complex environments. We currently have only an approximate function $P_{leave}(t)$. There are relatively few related studies about this phenomenon.

6.2 Arena with Obstacles

It is shown that the length of the obstacle influenced the aggregation speed and ratio in the global optimal source on the right-hand side. The larger the obstacle,

the slower the aggregation speed of the robot. It also affected the peak value of the number of aggregated robots in the local optimum on the left hand side.

It was unexpected that the presence of an obstacle, under certain circumstances, had a positive impact on the aggregation size. For example, in the group with $N = 200$ robots, the final aggregation performance in small obstacle experiments, $L_o \in \{36\%, 60\%\}$ were better than those in without obstacles. Our view is that the obstacle reduced the possibility for free robots on the right-hand side to leave the area.

On the other side, the number of robots was not always a positive factor for aggregation. In the experiments with 84% and 92% obstacles, the group with $N = 300$ robots performed worse than the one with $N = 200$ robots. That observed behaviour showed the higher the number of robots in the arena, the fewer the number of robots that can cross the passages (on top and bottom) made by the long obstacle. We observed the different stages of the experiment and found that the robots continually hovered near the passage, thereby reducing the possibility of other robots crossing the obstacle.

6.3 BEECLUST Algorithm in Complex Environment

The BEECLUST algorithm performed efficiently in the dual-cue environment with no obstacle, which was also reported in previous studies [8,31]. It coordinated individuals in the arena to find a global optimal source by following simple inter-robot interactions. Furthermore, when there were obstacles in the arena, the algorithm helped robots to successfully overcame the obstacle. Although the robots took longer to reach the peak of aggregation size in the arena with obstacle, the final aggregation size were similar to the no-obstacle configuration.

However, we have not observed if the algorithm can overcome a very complex situation e.g. a large obstacles during the specific experiment time, $t = 3600$ s. It still showed a trend that robots attempted to aggregate towards the global optimal source.

6.4 Simulation Platform: Bee-Ground

Our experiments proved that our simulation platform, Bee-Ground, is an efficient, flexible and realistic platform for the simulation of swarm robotic scenarios. It is an open-source platform [1] on GitHub. This platform is suitable for simulating more complicated environments such as a continuously changing environment and multiple cues.

7 Conclusion

A bio-inspired aggregation scenario, BEECLUST, was utilised to implement a bio-inspired swarm aggregation. The results showed that although the BEECLUST algorithm is a simple system, it was a successful algorithm in controlling a large swarm in a complex environment. The results demonstrated the

feasibility of the aggregation in finding the global optimal source in the presence of multiple sources. It was illustrated that the robots could overcome a certain degree of environmental complexities, thanks to the robustness of swarm systems. Meanwhile, in a complex environment with limited access, the swarm population was not always a positive factor to the final aggregation size at the global optimal source. For the future work, we will investigate effects of multi-layer environmental complexity using real robots. Also, a probabilistic macroscopic model based on [32] will be proposed to predict the collective behaviour of the swarm with additional environmental factors.

Acknowledgment. This work was partially supported by the UK EPSRC RAIN (EP/R026084/1), RNE (EP/P01366X/1), and the Field of Excellence COLIBRI of the University of Graz projects.

References

1. Bee-Ground: Open-sourced simulation tool for aggregation of robotics swarms. https://github.com/wshiyi-cn/BeeGround. Accessed 15 Jan 2020
2. Vensim^{TM}. http://www.vensim.com. Accessed 15 Jan 2020
3. Arvin, F., Espinosa, J., Bird, B., West, A., Watson, S., Lennox, B.: Mona: an affordable open-source mobile robot for education and research. J. Intell. Robot. Syst. **94**(3–4), 761–775 (2019)
4. Arvin, F., Murray, J., Zhang, C., Yue, S.: Colias: an autonomous micro robot for swarm robotic applications. Int. J. Adv. Robot. Syst. **11**, 1 (2014)
5. Arvin, F., Turgut, A.E., Bellotto, N., Yue, S.: Comparison of different cue-based swarm aggregation strategies. In: Tan, Y., Shi, Y., Coello, C.A.C. (eds.) ICSI 2014. LNCS, vol. 8794, pp. 1–8. Springer, Cham (2014). https://doi.org/10.1007/978-3-319-11857-4_1
6. Arvin, F., et al.: ΦClust: pheromone-based aggregation for robotic swarms. In: IEEE/RSJ International Conference on Intelligent Robots and Systems (IROS), pp. 4288–4294 (2018)
7. Arvin, F., Turgut, A.E., Krajník, T., Yue, S.: Investigation of cue-based aggregation in static and dynamic environments with a mobile robot swarm. Adapt. Behav. **24**(2), 102–118 (2016)
8. Arvin, F., Turgut, A.E., Krajník, T., Yue, S.: Investigation of cue-based aggregation in static and dynamic environments with a mobile robot swarm. Adapt. Behav. **24**(2), 102–118 (2016). https://doi.org/10.1177/1059712316632851
9. Bodi, M., Thenius, R., Szopek, M., Schmickl, T., Crailsheim, K.: Interaction of robot swarms using the honeybee-inspired control algorithm beeclust. Math. Comput. Model. Dyn. Syst. **18**(1), 87–100 (2012)
10. Brambilla, M., Ferrante, E., Birattari, M., Dorigo, M.: Swarm robotics: a review from the swarm engineering perspective. Swarm Intell. **7**, 1–41 (2013). https://doi.org/10.1007/sd11721-012-0075-2
11. Camazine, S., Deneubourg, J.L., Franks, N.R., Sneyd, J., Bonabeau, E., Theraula, G.: Self-organization in Biological Systems. Princeton University Press, Princeton (2003)
12. Caverzasi, E., Godin, A.: Stock-flow consistent modeling through the ages. Levy Economics Institute of Bard College Working Paper, no. 745 (2013)

13. Correll, N., Martinoli, A.: Modeling self-organized aggregation in a swarm of miniature robots. In: IEEE International Conference on Robotics and Automation: Workshop on Collective Behaviors inspired by Biological and Biochemical Systems (2007)
14. Frank, D., Jouandet, G., Kearney, P., Macpherson, L., Gallio, M.: Temperature representation in the drosophila brain. Nature **519**, 358–361 (2015). https://doi.org/10.1038/nature14284
15. Gauci, M., Chen, J., Li, W., Dodd, T.J., Groß, R.: Self-organized aggregation without computation. Int. J. Robot. Res. **33**(8), 1145–1161 (2014)
16. Grünbaum, D., Okubo, A.: Modeling social animal aggregations. In: Levin, S.A. (ed.) Frontiers in Mathematical Biology. Lecture Notes in Biomathematics, vol. 100, pp. 296–325. Springer, Heidelberg (1994). https://doi.org/10.1007/978-3-642-50124-1_18
17. Heran, H.: Untersuchungen über den Temperatursinn der Honigbiene (Apis mellifica) unter besonderer Berücksichtigung der Wahrnehmung strahlender Wärme. J. Comparat. Physiol. **34**, 179–206 (1952). https://doi.org/10.1007/BF00339537
18. Holland, O., Melhuish, C.: An interactive method for controlling group size in multiple mobile robot systems. In: 8th International Conference on Advanced Robotics, pp. 201–206 (1997)
19. Hu, C., Arvin, F., Xiong, C., Yue, S.: Bio-inspired embedded vision system for autonomous micro-robots: the LGMD case. IEEE Trans. Cogn. Dev. Syst. **9**(3), 241–254 (2016)
20. Krajník, T., et al.: A practical multirobot localization system. J. Intell. Robot. Syst. **76**(3–4), 539–562 (2014)
21. Krestovnikov, K., Cherskikh, E., Ronzhin, A.: Mathematical model of a swarm robotic system with wireless bi-directional energy transfer. In: Kravets, A.G. (ed.) Robotics: Industry 4.0 Issues & New Intelligent Control Paradigms. SSDC, vol. 272, pp. 13–23. Springer, Cham (2020). https://doi.org/10.1007/978-3-030-37841-7_2
22. Kube, C.R., Zhang, H.: Collective robotics: from social insects to robots. Adapt. Behav. **2**(2), 189–218 (1993)
23. Mermoud, G., Matthey, L., Evans, W.C., Martinoli, A.: Aggregation-mediated collective perception and action in a group of miniature robots. In: International Conference on Autonomous Agents and Multiagent Systems, pp. 599–606 (2010)
24. Michel, O.: Cyberbotics LTD. webots^{TM}: professional mobile robot simulation. Int. J. Adva. Robot. Syst. **1**(1), 5 (2004)
25. Na, S., et al.: Bio-inspired artificial pheromone system for swarm robotics applications. Adapt. Behav. 1–21 (2020). https://doi.org/10.1177/1059712320918936
26. Pinciroli, C., et al.: ARGoS: a modular, parallel, multi-engine simulator for multi-robot systems. Swarm Intell. **6**(4), 271–295 (2012)
27. Şahin, E.: Swarm robotics: from sources of inspiration to domains of application. In: Şahin, E., Spears, W.M. (eds.) SR 2004. LNCS, vol. 3342, pp. 10–20. Springer, Heidelberg (2005). https://doi.org/10.1007/978-3-540-30552-1_2
28. Schmickl, T.: How to engineer robotic organisms and swarms? In: Meng, Y., Jin, Y. (eds.) Bio-Inspired Self-Organizing Robotic Systems. Studies in Computational Intelligence, vol. 355, pp. 25–52. Springer, Heidelberg (2011). https://doi.org/10.1007/978-3-642-20760-0_2
29. Schmickl, T., Hamann, H.: BEECLUST: a swarm algorithm derived from honeybees. In: Bio-inspired Computing and Communication Networks, pp. 95–137 (2011)

30. Schmickl, T., Hamann, H., Wörn, H., Crailsheim, K.: Two different approaches to a macroscopic model of a bio-inspired robotic swarm. Robot. Auton. Syst. **57**(9), 913–921 (2009)
31. Schmickl, T., et al.: Get in touch: cooperative decision making based on robot-to-robot collisions. Auton. Agent. Multi-Agent Syst. **18**(1), 133–155 (2009)
32. Soysal, O., Sahin, E.: Probabilistic aggregation strategies in swarm robotic systems. In: Proceedings 2005 IEEE Swarm Intelligence Symposium, SIS 2005, pp. 325–332. IEEE (2005)
33. Turgut, A.E., Çelikkanat, H., Gökçe, F., Şahin, E.: Self-organized flocking in mobile robot swarms. Swarm Intell. **2**(2–4), 97–120 (2008)
34. Vaughan, R.: Massively multi-robot simulation in stage. Swarm Intell. **2**(2–4), 189–208 (2008)